

Reconstruction of permittivity images from capacitance tomography data by using very fast simulated annealing

C Ortiz-Aleman, R Martin and J C Gamio

Instituto Mexicano del Petroleo, Eje Central L Cardenas Nte #152, DF, CP 07730, Mexico

Received 22 December 2003, in final form 4 May 2004

Published 16 June 2004

Online at stacks.iop.org/MST/15/1382

doi:10.1088/0957-0233/15/7/022

Abstract

In this paper we introduce an image reconstruction technique for imaging permittivity distributions using electrical capacitance tomography, based on global optimization by very fast simulated annealing. Electrical capacitance measurement data are obtained between electrodes placed around the outer wall of an electrically insulating pipe. Such data are used to infer material distributions inside the pipe. The data are processed in order to reconstruct an image of the spatial distribution of the relative electrical permittivity (also known as dielectric constant) inside the pipe, which reflects a material distribution. In the very fast simulated annealing method, the permittivity image is reconstructed by minimizing iteratively a cost function related to the difference between the measured data and those calculated for an estimated permittivity distribution that is repeatedly updated, in a semi-random search process that mimics the thermodynamic phenomena of annealing (as metals slowly cool down) or crystallization (as liquids freeze). The images are refined until their calculated capacitance data match the measured data, in which case it is considered that such images properly resemble the permittivity distribution that produced the measured capacitance data.

Keywords: capacitance measurement, very fast simulated annealing, image reconstruction, finite volume method, tomography

Nomenclature

List of symbols

c	vector of mutual capacitances	ϕ^j	electrostatic potential distribution generated when electrode j is the source
c_{ij}	mutual capacitance coefficients	K_i	perturbation constant associated with each parameter
c_i	capacitance measured with electrode pair i	Γ_i	closed curve surrounding electrode i
dl	normal vector representing an element of the curve Γ	L	electrode length
ΔE	change in the system's total energy	L	'regularization' matrix
E	system's total energy or misfit function	N_r, N_θ	number of sections into which the radius and the circumference are divided
ϵ	vector of permittivities	N_T	maximum number of iterations in the inversion process
ϵ_0	permittivity of free space	q_i	induced electrode charges
$\epsilon(x, y)$	spatial distribution of the dielectric constant inside the sensor	T	temperature of the system
		T_0	initial temperature of the system
		v_i	electrode potentials

Abbreviations

ECT	electrical capacitance tomography
FEM	finite element method
FVM	finite volume method
GA	genetic algorithms
LBP	linear back projection
SA	simulated annealing
VFSA	very fast simulated annealing

1. Introduction

Electrical capacitance tomography (ECT) is a technique for obtaining cross-sectional images of the electrical permittivity distribution inside an electrically non-conducting body or region [1–4]. In a capacitance tomography system (figure 1), the sensor employed is made of a circular array of electrodes distributed around the cross-section to be examined. The mutual capacitance between all the different electrode-pair combinations is measured and, with the help of a computer and a suitable image reconstruction algorithm, this information is used to create a map showing the variation of the dielectric constant (or relative permittivity) inside the sensor area, thus providing an indication of the physical distribution of the various components of the mixture. For an n -electrode sensor, there are $m = \frac{1}{2}n(n - 1)$ possible electrode-pair combinations, and thus m independent mutual capacitance values. The electrodes are normally located on the outside of a non-conducting pipe, thus avoiding direct contact with the process fluids. A second external grounded metallic pipe (not shown in the figure) serves as an electric screen and to provide mechanical resistance. ECT has potential applications to imaging, monitoring and controlling numerous industrial multiphase processes. In particular, gas–oil two-phase flow measurement is an important application of ECT pertaining to the oil industry [5, 6].

However, so far the main limiting factor to the practical application of ECT has been the lack of fidelity or accuracy of the images obtained using the available image reconstruction methods [7]. Simple direct methods such as linear back-projection (LBP) yield relatively poor images that only provide a qualitative indication of the component distribution inside the sensor. On the other hand, more sophisticated methods, based on iterative local optimization techniques, generally require one or more regularization parameters whose optimal value depends precisely on the (unknown) image to be reconstructed, apart from the fact that the regularization employed has the

undesirable effect of smoothing the image contours, making it more diffuse. Thus, better and more accurate image reconstruction methods are still being developed in the context of this application.

The problem of calculating the mutual capacitances corresponding to a specific permittivity distribution inside the sensor is referred to as the forward problem. Conversely, the problem of estimating the spatial permittivity distribution inside the sensor that corresponds to a specific set of mutual capacitance values is referred to as the inverse problem, and is the problem that the image reconstruction methods must address and solve. Normally, the permittivity estimation is made in a spatially discrete way, representing it as a vector ε , which must be calculated from a vector \mathbf{c} of the m observed mutual capacitances, obtained using a suitable measurement apparatus. The size of ε is p , which is equal to the number of discrete regions (or pixels) into which the inside of the sensor is divided in order to form an image.

In order to solve the inverse problem, most ECT systems employ the LBP algorithm [4, 7–9], which is simple and fast. However, the LBP is based on making a linear approximation to a problem that is essentially nonlinear [10]. Therefore, this image reconstruction method causes considerable errors, which are particularly grave if there are large differences in permittivity within the image. So far, the main alternative to LBP has been the use of iterative methods that seek to minimize some objective function, employing local deterministic optimization techniques such as the regularized Newton–Raphson method or other similar approaches such as Landweber iteration [7, 11, 12]. These methods are based on iteratively minimizing with respect to ε the functional (or a similar one)

$$\|\mathbf{c}_{\text{meas}} - \mathbf{c}_{\text{calc}}\|^2 + \alpha^2 \|\mathbf{L}\varepsilon\|^2 \quad (1)$$

where α is a regularization parameter, \mathbf{L} is a ‘regularization’ matrix containing some type of *a priori* smoothness information about ε , and $\mathbf{c}_{\text{calc}} = \mathbf{f}(\varepsilon)$ is the vector of m calculated mutual capacitance values for a given permittivity distribution inside the sensor.

However, these image reconstruction methods have the problem that they require, for their correct operation, one or more regularization parameters whose proper value is strongly dependent, precisely, on the image that one wishes to reconstruct, implying that one would need to know beforehand the solution to the problem. Moreover, these methods produce distorted images, because the regularization has an excessive smoothing effect on the obtained permittivity. If the regularization is too strong the smoothing effect will occur, and if it is too weak the method can become unstable and/or not converge to the desired solution. These local optimization algorithms, during their search, explore only a relatively small sector of the solution domain, restricted to the vicinity of the initial guess. If the optimal solution of the problem, i.e., the absolute minimum of the objective function, is located far from the initial guess, it will be hard to reach due to the presence of relative minima in the way, places where these methods can become trapped. The most used methods in this category are least-squares linear inversion and techniques that utilize the gradient of the objective function, such as the steepest-descent and the conjugate-gradient methods. In general, local

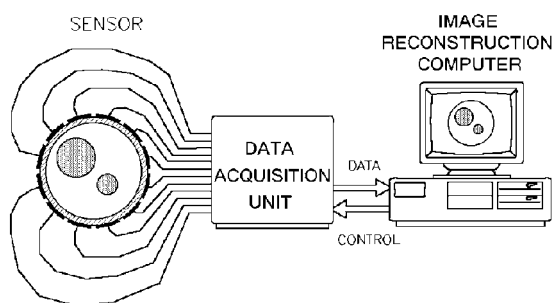


Figure 1. ECT system.

search methods exploit the scarce information derived from the comparison of a small number of models, thus avoiding an extensive search in the whole model space [13].

Global optimization methods explore the whole solution domain during the inversion process. They carry out an extensive scan within the model space. In this way, despite the existence of partial solutions to the problem, there is a greater possibility that the final solution corresponds to the best fit between the observed and the synthetic data. This type of method, in contrast to local techniques, does not require the information provided by the derivatives of the objective function, because in this case the problem does not need to be linearized. Global optimization algorithms use stochastic criteria in order to simultaneously explore all the solution space in search of the optimal model. The best known of the global methods is Monte Carlo, which performs a purely random and unbiased search. In other words, when generating each new model, it does not take advantage of the information obtained from the previously evaluated models [14]. The unguided randomness is the most characteristic feature of this method, which distinguishes it from the rest of the global methods. Among the global optimization techniques, there are also the methods of very fast simulated annealing (VFSA) and genetic algorithms (GA). Both were conceived as analogies of optimization systems occurring in nature. GA emulate the mechanisms of biological evolution while VFSA is based on thermodynamics. Both methods are inherently nonlinear and, therefore, lend themselves naturally to their application in capacitance tomography, a nonlinear problem. In the following sections, the application of VFSA to ECT image reconstruction is described. Reconstructed images are presented for a number of test cases representing typical two-phase flow patterns. These images are compared with those obtained using both LBP and Landweber iteration.

2. The very fast simulated annealing method

The VFSA method [15] is based on an analogy with the thermodynamic process of crystallization. A mineral fluid that cools slowly until it reaches a low-energy state, gives rise to the formation of well-defined crystals. If, in contrast, the substance leaves its thermal equilibrium state with a sudden or partial cooling, the resulting crystal will have many defects, or the substance may even form a ‘glass’, characterized by its meta-stable molecular disorder. This concept is used in the context of optimization methods to recognize potentially useful models or configurations.

The atoms of each molecular configuration are equivalent to the model parameters in the inverse problem (i.e., the permittivity of the various image pixels). The system energy for such a configuration is related to the cost (or misfit) function associated with the set of parameters involved in the model. In our case, the system energy is associated with the following L_2 norm

$$E = L_2 = \frac{\sum_{i=1}^m [c(i)_{\text{meas}} - c(i)_{\text{calc}}]^2}{\sum_{i=1}^m [c(i)_{\text{meas}}]^2} \quad (i = 1, \dots, m) \quad (2)$$

where $c(i)_{\text{meas}}$ are the m measured capacitances and $c(i)_{\text{calc}}$ are the ones calculated by solving the forward problem for a given

permittivity distribution ϵ . This form of the energy term is often used and has proved to be very effective in applications where physical properties are sought from the inversion of real measured data [13].

In this work, the forward problem was solved using the finite-volume method (FVM), which is described in the appendix. From an initial permittivity distribution, the method generates a range of configurations or parameter (permittivity) combinations considering a certain temperature T for the process. For this purpose the Metropolis *et al* [16] criterion is employed, which consists in changing a parameter, in each iteration, by a small random amount. This shift causes a change ΔE in the system’s total energy. If ΔE is less than or equal to zero, the change in the parameter is accepted and the resulting configuration is considered as the new current configuration. When there is an increase in the system energy (ΔE is greater than zero), the probability of acceptance or rejection for the parameter change is determined as

$$P(\Delta E) = e^{-\Delta E/T}. \quad (3)$$

In order to decide whether or not a change that produces an increase in the system energy is accepted, a random number between zero and one is chosen, which is then compared with the value of the probability corresponding to ΔE . If the said random number is smaller, the parameter shift is accepted and the new configuration is considered as the current (updated) one. If the said random number is greater, the parameter shift is not accepted and the configuration that existed before the shift is maintained. Repeating this procedure continuously, the thermal movement of the atoms of a system in thermal equilibrium (at a fixed temperature T) is simulated. In order to reach the system’s base state, that is to say, the state of lowest energy and highest order, the temperature for each parameter must be reduced very slowly, simulating a quasi-static process. This means that, during the cooling, the system must experience a series of states infinitesimally separated from the state of thermal equilibrium.

The method of VFSA has three basic components [15]: an energy (or cost, or misfit) function, an order function (the Metropolis criterion), and a set of parameters that control the temperature for each model parameter. The process consists of three nested cycles. Figure 2 shows a diagram that illustrates how the method works.

The external cycle (3) regulates the system temperature. Every time a cycle is completed, the temperature for each parameter decreases as its initial temperature is multiplied by an exponential factor that depends on a control parameter c (which helps tune the algorithm for specific problems), and N which is the number of model parameters. In this way the desired slow and gradual cooling is carried out. The intermediate cycle (2) updates the values, independent of each other, of a series of constants K_i associated with each parameter. Said constants determine the maximum change that each parameter may experience when it is perturbed in the innermost cycle (1). The values of the said constants depend on the number of times that the current model has been accepted (according to the Metropolis criterion) at the end of every sequence of internal cycles (1). In the internal cycle (1) the parameter values are perturbed using the factors K_i , defined in the intermediate cycle (2). The perturbation is done

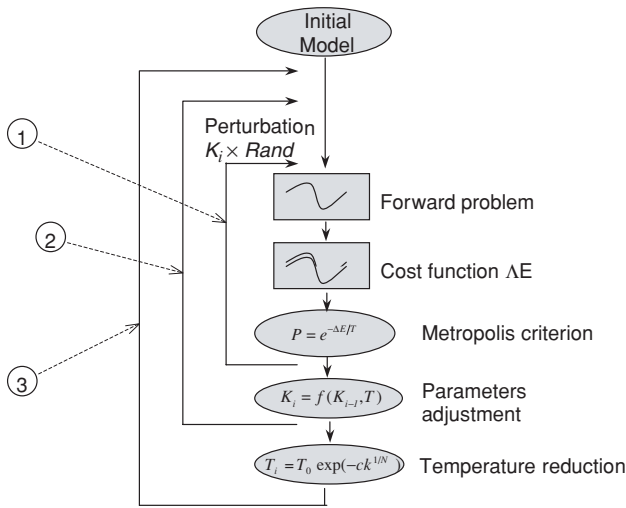


Figure 2. Schematic diagram of the VFSA method.

multiplying each parameter by the product of its corresponding K_i times a randomly chosen number between minus one and one. After this, the synthetic response of the current model is calculated and the change in the system's energy associated with the new parameter configuration is evaluated. The said energy change corresponds to the misfit between the synthetic data curve and the observed or measured one. If the misfit decreases, then the new configuration will be accepted as the current one and in turn perturbed in the same way. If, in contrast, the random perturbation causes an increase in the misfit, associated with an increment in the energy E , then that configuration is assigned a probability of acceptance according to the Metropolis criterion.

Cycles (1), (2) and (3) are repeated, while the temperature of the process decreases progressively. As the temperature diminishes, the parameter variations are smaller and smaller. In this way, the search in the solution domain tends to confine itself towards the models associated with the absolute minimum of the misfit function E . The end result is a set of values for the parameters (i.e., the permittivity in the various pixels that make an image) whose synthetic response reproduces the observed (capacitance) data, with a sufficiently small error.

As an example, one possible specific embodiment of, albeit not the only one, the method of simulated annealing is presented in figure 3. The method starts in block (1), with a series of initial values for the temperature, the perturbation constants, the permittivities and the cost or misfit function (T_0 , $K_{i(0)}$, $\varepsilon_{i(0)}$ (with $i = 1, \dots, p$) and E_0), and initializing the external cycle counter, denoted by k . Next, in block (2) the counters for the internal and intermediate cycles, i and j , are initialized, and the internal cycle starts. In it, one by one the parameters (or permittivities) are subject to a random perturbation in block (3). Still in block (3), each time a parameter is perturbed, the forward problem is solved and the cost or misfit function, E , is calculated applying equation (2). If there was a decrease of E with respect to the previous evaluation of it, the perturbed parameter value is accepted as the new current value, the internal cycle parameter counter i is increased by one, and the method proceeds to

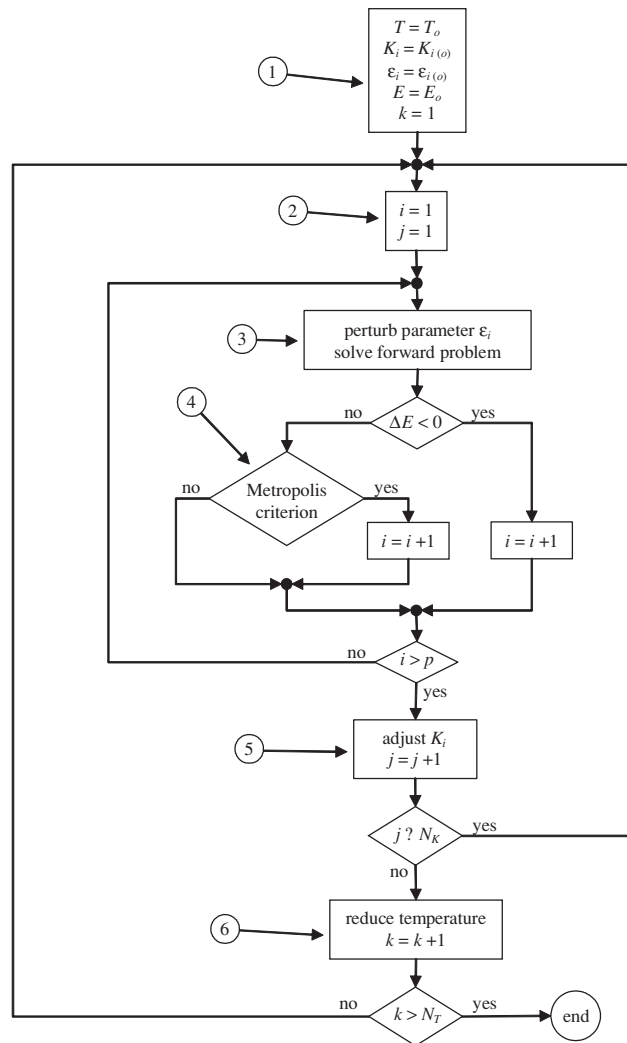


Figure 3. One possible implementation of the VFSA.

perturb the next parameter (if there is one). If, in contrast, there was an increase in E , then the Metropolis criterion is applied, in block (4), in order to decide whether or not the perturbed parameter value is accepted as the new current one. If, according to said criterion, the new value is accepted, then the internal cycle counter i is incremented by one and the method proceeds to perturb the next parameter (if there is one). If, according to the Metropolis criterion, the perturbed value is not accepted, then the counter i is not incremented and the method proceeds to perturb once again the same parameter. Once all parameters ε_i have been updated, in block (5) the values of the constants K_i (which determine how the parameters are perturbed within the internal cycle) are adjusted, and the intermediate cycle counter j is increased by one. N_K determines how many times the internal cycle will be repeated without reducing the temperature of the system. In other words, the intermediate cycle consists in the repetition of the internal cycle N_K times, but with different values for K_i . This is done in order to prevent the temperature for each parameter from descending too fast, which can have negative effects in some VFSA applications. However, in our particular case that does not happen, and the value of N_K is taken as one. At the end of the intermediate cycle, in block (6) the temperature for each

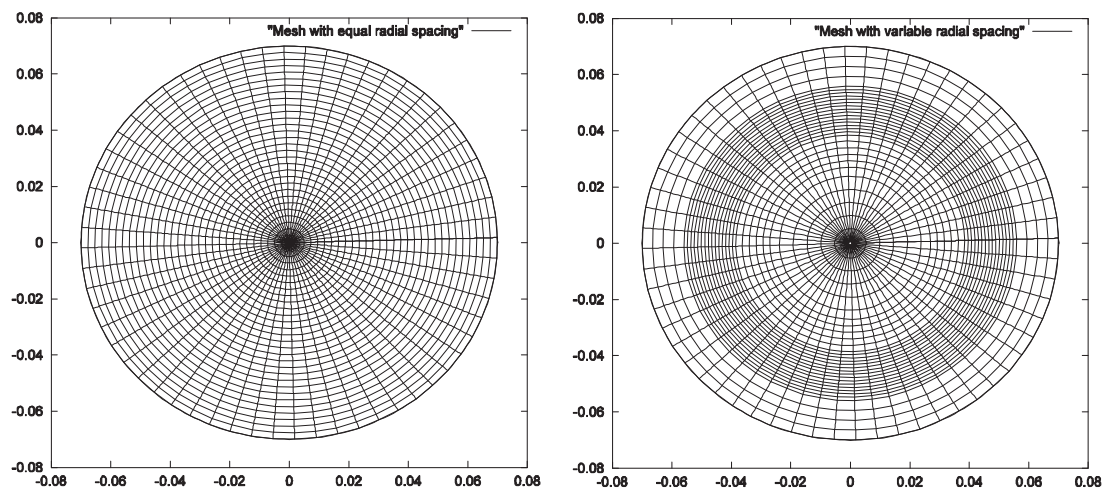


Figure 4. Mesh with equal radial spacing (left) as employed in [17] and mesh with variable radial spacing used in this work (right).

parameter is reduced as indicated in previous paragraphs and the external cycle counter k is increased by one. The whole previous procedure is repeated until k reaches the iteration limit N_T , or before that if a sufficiently low value for the cost function E is obtained.

In the context of global optimization methods such as VFSA, spatial regularization schemes are used in order to reduce the number of parameters involved in the inversion (the permittivities in our case), based on an efficient interpolation strategy. In this work, bicubic spline interpolation was used on the permittivity distributions. Through this approach, it was possible to perform the inversion of the capacitance data using only 240 parameters to represent the permittivity distribution, instead of the full 240×120 discretization used in the sensor model (see the following section).

3. Results and discussion

In a previous work [17], we tested the feasibility of both GA and the standard simulated annealing (SA) method by computing sets of synthetic ECT data for typical permittivity distributions using our FVM forward problem routine. A 240×120 polar grid was employed in the forward problem solution to simulate a 12-electrode ECT sensor. We considered two-component distributions, with air ($\varepsilon = 1$) as the lower permittivity material and oil ($\varepsilon = 2.5$) as the higher permittivity material. In the first two cases (annular and stratified flows), the numerical test was restricted to the reconstruction of noise-free ECT data. In a third case (bubbly flow) a random noise level of 5% was added to the capacitance data. In all cases, after an appropriate parametrization, both methods produced similar results and the quality of the reconstructed permittivity images was mainly dependent on the number of forward problem calculations (i.e., the number of iterations). In this way, the SA method was validated for synthetic models as well as for noisy synthetic data.

In this paper we apply the VFSA method to both synthetic (simulated) and measured ECT data. We decided to use VFSA as it has recently been found to be computationally much more efficient than SA.

At a first stage, before applying the VFSA method, we compared our FVM calculated data with the measured

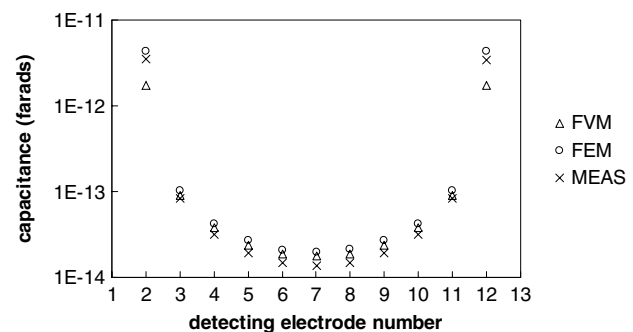


Figure 5. Comparison of measured and calculated (using both FVM and FEM) capacitance data between electrode 1 and each one of the others (2 to 12) for an empty 12-electrode ECT sensor with 10 cm long electrodes.

ECT data for an empty sensor (homogeneous distribution with permittivity of air). We used a grid of the same size (240×120) as the one previously employed in [17], but we made some changes in order to refine in the vicinity of the electrodes. In order to improve the accuracy of capacitance calculation, the mesh is refined along the radial direction in an annular region including the electrodes. Making a compromise between fewer mesh points in both the inner region of the mesh and close to the outer screen, and more points close to the electrodes, accuracy is better achieved in capacitance calculation with this new mesh for the same number of mesh points. Both kinds of meshes are depicted in figure 4.

As can be seen in figure 5, calculated capacitances are not equal to measured capacitances: there exist some differences, especially when the measurement electrode is closer to the source electrode. In the case of the FVM approach used in this work, we only found major difficulties when the source and measurement electrodes are neighbours. In order to make both sets of data comparable, a series of calibration factors for each measurement electrode was inverted using the VFSA method. These factors are multiplicative constants (incorporated as model parameters in the inversion) that produced the best fit between the observed and calculated capacitance data sets for an empty sensor. In this way, at the cost of some loss of resolution, we avoided the use of a finer and larger grid in the

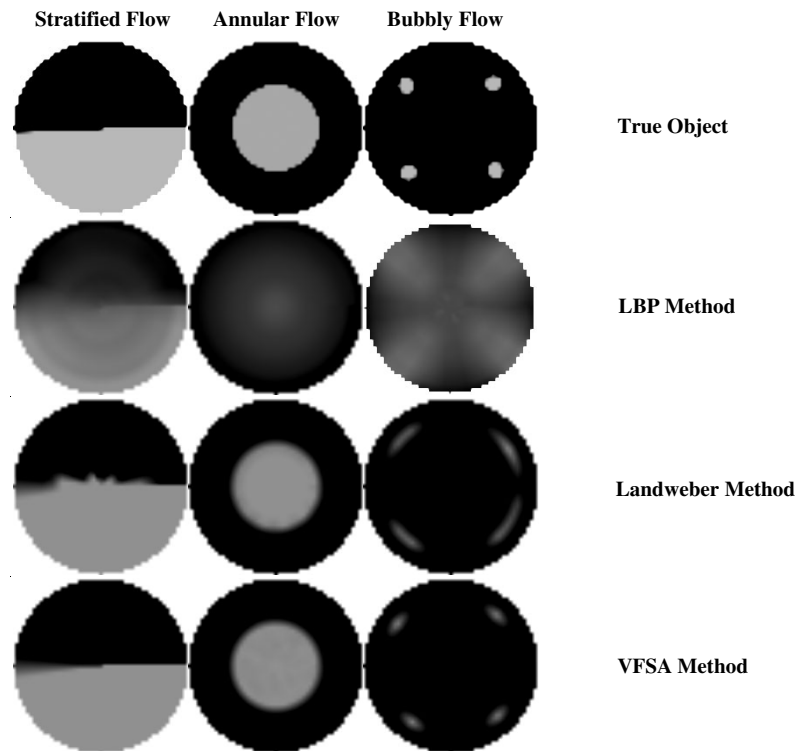


Figure 6. Image reconstruction of synthetic ECT data for three test distributions. Reconstructed images after 1000 iterations of projected Landweber and VFSA methods. Black and white represent the permittivity of a nylon pipe and air, respectively.

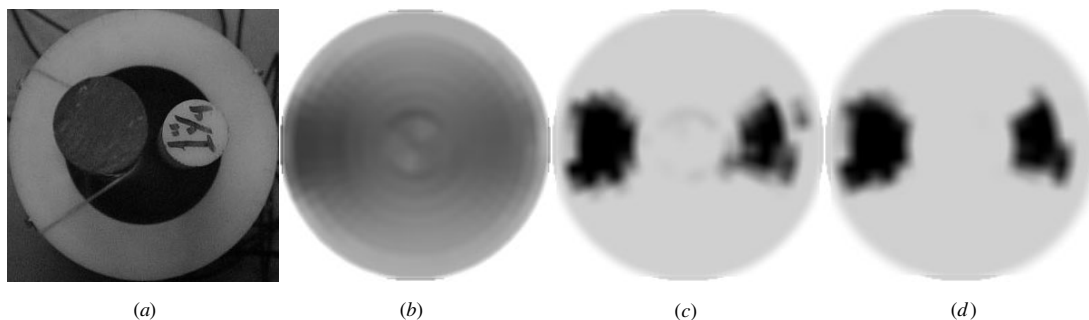


Figure 7. Image reconstruction of measured ECT data: (a) distribution of true objects (a perpex rod and a nylon rod) inside the sensor; (b) LBP reconstructed image; (c) reconstructed image after 500 iterations of projected Landweber and (d) VFSA reconstruction after ~ 300 iterations. Landweber's solution was used as a starting model for the VFSA method. Black and white represent the permittivity of rods and air, respectively.

forward problem computation. Another possibility, which was also tested and found worse than the one just described above, is to disregard the two data points corresponding to the cases of measurement electrodes adjacent to the source electrode (since these were the ones that presented the largest error). Note in figure 5 that the data yielded by FVM are closer to the actual measurements compared to FEM, except for the case of adjacent electrodes, which is dealt with through the use of the calibration factors mentioned above.

In order to assess the image reconstruction performance of VFSA with the simulated data, the method was applied to three test cases representing typical stratified, annular and bubbly two-phase flow patterns. A homogeneous distribution with the permittivity of air was used as an initial model and two thousand iterations were employed. The resulting images are shown in figure 6, where they are compared with those

obtained using both straight LBP and the Landweber iteration method (with one thousand iterations). The VFSA images appear to reproduce better the true image in a similar number of iterations. The spatial image error [18] was used as a figure of merit, defined as

$$\delta = \frac{\sum_{i=1}^p |\varepsilon_{i(\text{img})} - \varepsilon_{i(\text{ref})}|}{\sum_{i=1}^p \varepsilon_{i(\text{ref})}}. \quad (4)$$

The spatial image error was computed for all images and is given in table 1. The results confirm the advantage of VFSA over the other reconstruction methods used.

Finally, the VFSA method was tested with actual measured data. In a first experiment, a perpex rod and a nylon rod were placed inside a real 12-electrode ECT sensor (see figure 7(a)), connected to the author's ECT system. Measured capacitance data from each electrode were properly corrected

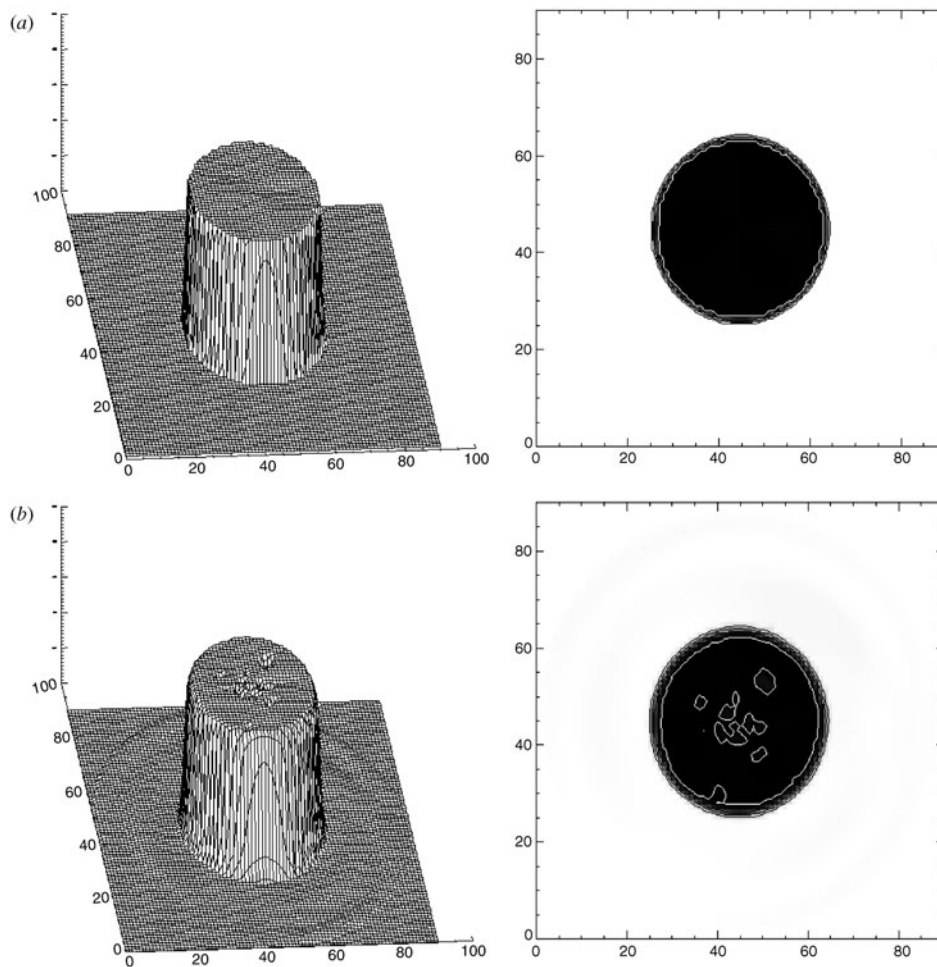


Figure 8. Image reconstruction of measured ECT data: (a) test distribution and (b) reconstructed image after 10 000 iterations of the VFSA method. Black and white represent the permittivity of a nylon pipe and air, respectively.

Table 1. Spatial image errors (equation (4)) and capacitance errors (equation (2)) for the reconstruction of synthetic ECT data (see figure 6).

	LBP (%)	Landweber (%)	VFSA (%)
Annular flow			
Image error	57.0	39.6	15.4
Capacitance error	3.3	2.5	0.6
Stratified flow			
Image error	28.7	20.8	14.3
Capacitance error	3.0	1.5	0.6
Bubbly flow			
Image error	9.2	5.7	4.3
Capacitance error	2.8	2.5	0.7

using the calibration factors described earlier. We used the permittivity distribution from the projected Landweber method as an initial model for the VFSA method, as this last method can be used as a postprocessing tool when real-time applications are required. The reconstruction of this permittivity distribution, after three hundred computations of the forward problem, is depicted in figure 7(d) along with the corresponding LBP and Landweber images (figures 7(b) and (c)). The associated capacitance errors are given in table 2. Note that in this case the VFSA method can improve

Table 2. Capacitance errors (equation (2)) for the reconstruction of measured ECT data (see figure 7).

	LBP (%)	Landweber (%)	VFSA (%)
Real data			
Capacitance error	4.5	2.6	0.6

Landweber’s reconstruction accuracy to an acceptable degree after just a few iterations.

As a consequence of a lower resolution in the computation of the forward problem (when using VFSA) and the sensitivity matrix (in the cases of LBP and Landweber methods), the images obtained here by VFSA were not fairly equivalent in terms of quality to those reported in [17], produced by GA and standard SA. The shape of the reconstructed objects is distorted as a consequence of the kind of patches we employed for the discretization. Nevertheless, application of VFSA, even in the case of measured data, can lead to high quality reconstructions by increasing the number of permittivity parameters in the forward problem computation and the number of iterations in the inversion process. In order to illustrate this last fact, we reconstructed a permittivity distribution resultant from placing a nylon rod at the centre of the ECT sensor. We used a homogeneous distribution with permittivity of air as the

initial model, as this method does not require a good starting model. Results after ten thousand computations of the forward problem are depicted in figure 8.

4. Conclusions

Application of VFSA to the inversion of measured and synthetic ECT data has provided us with encouraging results. In this work we followed the advice of Yang and Peng [7] to test nonlinear methods for both forward modelling (FVM) and reconstruction of electrical permittivity images by means of global inversion methods (VFSA).

One significant disadvantage of VFSA, relative to linear methods such as LBP, is its much higher computation time as it requires several hundreds of forward problem computations, which makes it unsuitable for real-time applications. However, for relatively slow processes or when off-line processing of the data is acceptable, VFSA is an attractive alternative for image reconstruction offering better accuracy than other methods. This nonlinear inversion method does not require a good starting model and has been found to be successful in inversion of permittivity images from the ECT data. The VFSA method has been validated using synthetic models as well as measured data. Thus, this approach can be used for routine interpretation of ECT data or alternatively as a post-processing tool in combination with the projected Landweber approach.

Acknowledgments

M Sen and A Iglesias are thanked for their very helpful advice on application of the VFSA method. This work was supported by projects IMP-D.00117 and IMP-D.00046.

Appendix. Forward problem solution

The forward problem consists in calculating the mutual capacitances c_{ij} , $i \neq j$, that result from the presence of a permittivity distribution ε inside the sensor. The VFSA method requires the repeated solution of the forward problem. Because of that, it is important to have a suitable method to solve said problem, which achieves a reasonable balance between accuracy (or precision) and speed. In this paper, the forward problem was solved using an optimized routine based on the finite-volume method (FVM), which will be described briefly. This routine is very efficient and comparable in its precision with implementations based on the finite-element method (FEM) using meshes with 9000 triangular elements. The routine is written in Fortran 90 and is highly portable.

The use of the cylindrical axial end guards in the sensor, and the assumption that the phase (and thus the permittivity) distribution does not change too much in the axial direction, allow the sensor to be represented by a two-dimensional (2D) model [8]. The forward problem is solved using the finite-volume method in a cylindrical configuration. In this way, the undetermined solutions at the centre of the disc (which are a problem in the finite-difference method) are eliminated and the mesh refinement becomes more flexible as compared

to finite-element methods. The following equation is solved in 2D

$$\nabla \cdot \varepsilon(x, y) \nabla \phi^j = 0 \quad (\text{A.1})$$

where ε is the permittivity and ϕ^j is the electrostatic potential distribution generated when electrode j is the source (or excitation). The equation is subject to the boundary conditions (a) $\phi^j = V$ (V) on the source electrode and (b) $\phi^j = 0$ on the detection electrodes and on the outer screen.

Defining the radial and angular coordinates as r and θ , and using the finite-volume method, the discrete equation is formulated in conservative form for each cell $\Omega_{\alpha\beta}$ as

$$\int_{\Omega_{\alpha\beta}} \nabla \cdot (\varepsilon \nabla \phi^j) d\Omega_{\alpha\beta} = 0 \quad \text{for } \alpha = 1, \dots, N_r \quad \text{and} \\ \beta = 1, \dots, N_\theta \quad (\text{A.2})$$

where the indices α and β refer to the discretizations in r and θ , respectively, and N_r and N_θ are the numbers of sections into which the radius and the circumference are divided, respectively.

Applying Gauss's theorem in polar coordinates, the discrete equations can be written as

$$\int_{\Gamma_{\alpha\beta}} \varepsilon \nabla \phi^j \cdot d\Gamma_{\alpha\beta} = 0 \quad (\text{A.3})$$

where $\Gamma_{\alpha\beta}$ is the boundary of the finite volume cell $\Omega_{\alpha\beta}$. The boundary $\Gamma_{\alpha\beta}$ is defined by Γ_W and Γ_E along the radial coordinates, and by Γ_N and Γ_S along the angular coordinates. Equation (A.3) can be expressed as the sum of the fluxes through the faces Γ_N , Γ_S , Γ_E and Γ_W

$$\sum_l \left(\int_{\Gamma_l} \varepsilon \nabla \phi^j \cdot n_l d\Gamma_l \right) \\ = \left(\frac{\varepsilon}{r} \frac{\partial \phi^j}{\partial \theta} \Delta r \right) \Big|_{(\alpha+\frac{1}{2}),\beta} - \left(\frac{\varepsilon}{r} \frac{\partial \phi^j}{\partial \theta} \Delta r \right) \Big|_{(\alpha-\frac{1}{2}),\beta} \\ + \left(\varepsilon \frac{\partial \phi^j}{\partial \theta} r \Delta \theta \right) \Big|_{\alpha,(\beta+\frac{1}{2})} - \left(\varepsilon \frac{\partial \phi^j}{\partial \theta} r \Delta \theta \right) \Big|_{\alpha,(\beta-\frac{1}{2})} \quad (\text{A.4})$$

From equation (A.4), the term corresponding to the fluxes at zero radius vanishes and the problem is equivalent to solving the equations in the proximity of the centre on triangles that have a vertex on the centre. Then, the discrete system of equations for the forward problem is well posed. The complete system is similar to a Laplacian system of equations, and a diagonal banded system that includes the periodic boundary conditions imposed by the problem geometry must be solved. The corresponding matrix is positive definite and non-symmetric, characteristics that were exploited when selecting the biconjugate gradient method for its solution.

Finally, the mutual capacitances were calculated by integrating the potential gradients along a curve surrounding the electrodes, the following equation,

$$\tilde{c}_{ij} = \frac{\tilde{q}_i}{v_j} = -\frac{\varepsilon_0}{V} \oint_{\Gamma_i} (\varepsilon \nabla \phi^j) \cdot d\mathbf{l} = -\frac{\varepsilon_0}{V} \oint_{\Gamma_i} \varepsilon \frac{\partial \phi^j}{\partial n} dl \quad (\text{A.5})$$

where \tilde{c}_{ij} is the capacitance per unit length between electrodes i and j , \tilde{q}_i is the electric charge per unit length induced on electrode j (the detection electrode), v_j is the voltage applied to electrode j (the source electrode), ε_0 is the permittivity

of free space ($8.854 \times 10^{-12} \text{ F m}^{-1}$), Γ_i is a closed curve surrounding electrode i , dl is a normal vector representing an element of the curve Γ_i , dl is an element of length of that curve and ϕ^j is the electrostatic potential distribution produced in the sensor when applying a voltage of V V to electrode j (source) and 0 V to all others (detection electrodes). The integration is done using a trapezoidal rule and the potential gradients were calculated to the fourth order. The total capacitances c_{ij} are obtained multiplying \tilde{c}_{ij} by the electrode length, 0.1 m in our case.

During the procedure for reconstructing a permittivity image using VFSA, it is necessary to solve the forward problem and find the electric potential repeatedly for relatively similar successive permittivity distributions, while the method converges towards the final solution. Since the potential corresponding to said successive distributions changes relatively little, it is possible to accelerate the whole process if an iterative method is used to solve the forward problem, taking as the first guess for the potential the solution potential corresponding to the previous permittivity configuration. Because the initial guess for the potential will be quite close to the solution, said iterative method will converge in fewer iterations, rapidly achieving an acceptable accuracy.

References

- [1] Williams R A and Beck M S (ed) 1995 *Process Tomography—Principles, Techniques and Applications* (Oxford: Butterworth Heinemann)
- [2] Beck M S, Byars M, Dyakowski T, Waterfall R, He R, Wang S M and Yang W Q 1997 Principles and industrial applications of electrical capacitance tomography *Meas. Control* **30** 197–200
- [3] Gamio J C 1997 A high-sensitivity flexible-excitation electrical capacitance tomography system *PhD Thesis* University of Manchester Institute of Science and Technology, UK
- [4] Plaskowski A, Beck M S, Thorn R and Dyakowski T 1995 *Imaging Industrial Flows: Applications of Industrial Process Tomography* (Bristol: Institute of Physics Publishing)
- [5] Thorn R, Johansen G A and Hammer E A 1997 Recent developments in three phase flow measurement *Meas. Sci. Technol.* **8** 691–701
- [6] Hammer E A and Johansen G A 1997 Process tomography in the oil industry: state of the art and future possibilities *Meas. Control* **30** 212–6
- [7] Yang W Q and Peng L 2003 Image reconstruction algorithms for electrical capacitance tomography *Meas. Sci. Technol.* **14** R1–13
- [8] Xie C G, Plaskowski A and Beck M S 1989 8-electrode capacitance system for two-component flow identification: part 1. Tomographic flow imaging *IEE Proc. A* **136** 173–83
- [9] Xie C G, Huang S M, Hoyle B S, Thorn R, Lenn C, Snowden D and Beck M S 1992 Electrical capacitance tomography for flow imaging: system model for development of image reconstruction algorithms and design of primary sensors *IEE Proc. G* **139** 89–98
- [10] Gamio J C and Ortiz-Aleman C 2003 An interpretation of the linear back-projection algorithm used in electrical capacitance tomography *Proc. 3rd World Congress on Industrial Process Tomography* pp 427–32
- [11] Yang W Q, Spink D M, York T A and McCann H 1999 An image-reconstruction algorithm based on Landweber's iteration method for electrical-capacitance tomography *Meas. Sci. Technol.* **10** 1065–9
- [12] Vauhkonen M, Lionheart W R B, Heikkinen L M, Vauhkonen P J and Kaipio J P 2001 A MATLAB package for the EIDORS project to reconstruct two-dimensional EIT images *Phys. Meas.* **22** 107–11
- [13] Sen M K and Stoffa P L 1995 *Global Optimization Methods in Geophysical Inversion* (Amsterdam: Elsevier)
- [14] Rodríguez-Zúñiga J L, Ortiz-Aleman C, Padilla G and Gaulon R 1996 Application of genetic algorithms to constrain shallow elastic parameters using *in situ* ground inclination measurements *Soil Dyn. Earth Eng.* **16** 223–34
- [15] Ingber L 1989 Very fast simulated re-annealing *Math. Comput. Modelling* **12** 967–73
- [16] Metropolis N, Rosenbluth A, Rosenbluth M, Teller A and Teller E 1953 Equation of state calculations by fast computing machines *J. Chem. Phys.* **21** 1087–92
- [17] Ortiz-Aleman C, Martin R and Gamio J C 2003 Application of simulated annealing and genetic algorithms to the reconstruction of electrical permittivity images in capacitance tomography *Proc. 3rd World Congress on Industrial Process Tomography* pp 794–9
- [18] Huang S M, Xie C G, Vasina J, Lenn C, Zhang B F and Beck M S 1993 Experimental evaluation of capacitance tomographic flow imaging systems using physical models *Tomographic Techniques for Process Design and Operation* ed M S Beck, E Campogrande, M Morris, R A Williams and R C Waterfall (Southampton: Computational Mechanics Publications) pp 347–60